Electronic Supplementary Material (ESI) for Journal of Materials Chemistry A.

Supporting Information

Isomeric Effects of Chlorinated End Groups on Efficient Solar Conversion

Daize Mo,[ab] [+] *Hui Chen,*[ac][+] *Jiadong Zhou,*[d][+] *Liang Han,*[a] *Yulin Zhu,*[a] *PengJie Chao,*[a] *Nan Zheng,*[d] *Zengqi Xie*[d] *and Feng He*[*ae]

[+]These authors contributed equally to this work.

*E-mail: hef@sustech.edu.cn (F.H.).

Characterization

^{1}HNMR spectra were recorded on a Bruker AV-500 spectrometer in deuterated chloroform solution at room temperature with tetramethylsilane (TMS) as the internal reference. The multiplicities of NMR signals were described as follows: s, singlet; d, doublet; t triplet; m, multiplet. Preparative gel permeation chromatography purification was performed with a JAI LC-9104 recycling preparative high performance liquid chromatography, and the eluent was chloroform. High resolution mass spectra were recorded on an Autoflex III matrix-assistedlaser desorption ionization mass spectrometer (MALDI-TOF-MS). Thermogravimetric analysis (TGA) plots were conducted on a Discovery series instrument under a nitrogen atmosphere with a heating rate of 10 °C /min in N_2. UV-Vis absorption spectra were recorded on the Shimadzu UV3600 spectrometer. For the solid state measurements, the **BTIC-2Cl-γ**, **BTIC-2Cl-δ**, and **BTIC-2Cl-β** solutions in chloroform were spin-coated on quartz plates. Cyclic voltammetry was performed on a Model CHI 660E potentiostat/galvanostat (Shanghai Chenhua Instrumental Co., Ltd. China) to determine the HOMO and LUMO levels of the monomers, in an dichloromethane solution of 0.1 mol L^{-1} tetrabutylammonium hexafluorophosphate(*n*-Bu_4NPF_6) at a potential scan rate of 100 mV s^{-1} with an Ag/Ag+ reference electrode and a platinum wire counter electrode under an argon atmosphere. The redox potential of ferrocene/ferrocene$^+$ (Fc/Fc^+) under the same conditions is located at 0.044 V, which is assumed to have an absolute energy level of -4.8 eV to vacuum. The HOMO and LUMO were calculated by the following equation: HOMO (eV) =-4.74+ φ_{ox},

LUMO(eV)=-4.74+φ_{red}. Where φ_{ox} is the onset oxidation potential *vs* Ag/Ag+ and φ_{red} is the onset reduction potential *vs* Ag/Ag^{+}. Atom force microscopy (AFM) images were taken on a NanoScopeIIIa controller (Veeco Metrology Group/Digital Instruments, Sant a Barbara, CA), using built-in software (version V6.13R1) to capture images. Transmission electron microscopy (TEM) images were acquired using a TEM Hitachi HT7700electron microscope operating at an acceleration voltage of 100 kV.

Device Fabrication and Testing

The ITO substrates were sonicated sequentially in acetone, detergent, deionized water and isopropyl alcohol to clean the ITO surface, followed by drying at 90 °C for overnight in vacuum oven. ZnO interlayer from precursor solution was spin-coated onto the pre-cleaned and UV-treated ITO substrates, and then heated at 200 °C for 1 hour. The device structures of ITO/ZnO/PBDB-TF: **BTIC-2Cl-γ** (**BTIC-2Cl-δ**/**BTIC-2Cl-β**)/MoO_3/Ag was fabricated. The polymers were co-dissolved in $CHCl_3$, at total solids concentration of 4 mg mL^{-1} and were stirred overnight at temperature of 70 °C. The active layer was spin-coated from the cooled blend solution obtain high neat films, part of them were treated by thermal annealing at 100 °C. Subsequently, the resulted active films were transferred into a vacuum chamber. Afterwards, 10 nm molybdenum oxide (MoO_3) hole buffer and 100 nm Ag electrode were deposited by thermal evaporation through a defined shadow mask in a vacuum chamber with a pressure of approximately 1×10^{-4} Pa. The completed devices were tested in closed glove box.

Characterization of device

Steady-state current-voltage (*J-V*) curves were measured by a Keithley 2400 source-measurement unit under AM 1.5 G spectrum from a solar simulator (Enlitech. Inc) calibrated by a silicon reference cell (Hamamatsu S1133 color, with KG-5 visible fiith). All EQE data were gained through the measurement of solar cell spectral response measurement system QE-R3011 (Enli Technology Ltd., Taiwan). The mobility of electron was tested by fitting the current-bias characteristics in dark utilizing a field-independent space charge limited current (SCLC) model following the Mott-Gurney law. Hole-only devices were fabricated with the device structure ITO/PEDOT: PSS/PM6: chlorinated acceptors/MoO_3/Ag. The mobility was determined by fitting the dark current to the model of a single carrier SCLC, which is described by the equation

$$J = \frac{9}{8}\varepsilon_0\varepsilon_r\mu_h\frac{V^2}{d^3}$$

where J is the current, μ_h is the zero-field mobility, ε_0 is the permittivity of free space, ε_r is the relative permittivity of the material, d is the thickness of the active layer, and V is the effective voltage. The effective voltage can be obtained by subtracting the built-in voltage (V_{bi}) and the voltage drop (V_s) from the substrate's series resistance from the applied voltage (V_{appl}), $V = V_{appl} - V_{bi} - V_{s.}$ The hole-mobility can be calculated from the slope of the $J^{1/2} \sim V$ curves.

Materials. The core unit BT-CHO, IC-Cl-δ, IC-Cl-γ, and IC-Cl-β were prepared by referencing the reported literature[1-3]. All other reagents and chemicals were purchased from the commercial sources and used without other further purification.

Synthesis of 2,2'-((2Z,2'Z)-((12,13-bis(2-ethylhexyl)-3,9-diundecyl-12,13-dihydro-[1,2,5]thiadiazolo[3,4-e]thieno[2'',3'':4',5']thieno[2',3':4,5]pyrrolo[3,2-g]thieno[2',3':4,5]thieno[3,2-b]indole-2,10-diyl)bis(methanylylidene))bis(5-chloro-3-oxo-2,3-dihydro-1H-indene-2,1-diylidene))dimalononitrile (BTIC-2Cl-γ). Compound **BT-CHO** (0.1036g, 0.1036mmol) and **IC-2Cl-γ** (0.109g, 0.414 mmol) were added into a 50 mL round bottom flask. After the flask was blanked by argon three times, chloroform (25 mL) was added via syringe at once and then pyridine (0.5 mL) was added slowly. After that, the mixture was refluxed at 70 °C overnight. The product was precipitated in 150 mL of methanol and then filtered. The crude product was purified with column chromatography on silica gel using $CHCl_3$ as the eluent to obtain the dark blue solid **BTIC-2Cl-γ** (0.142 g, 94.5% yield). ^{1}H NMR (400 MHz, $CDCl_3$) δ: 9.21 (s, 2H), 8.67 (d, *J* = 8 Hz, 2H), 7.91 (s, 2H), 7.15 (dd, *J* = 4 Hz, 2H), 4.79 (d, J = 8 Hz, 4H), 3.26 (t, J = 8 Hz, 4H), 2.12-2.10 (m, 2H), 1.95-1.87 (m, 4H), 1.56-1.50 (m, 4H), 1.42-1.11 (m, 30H), 1.10-1.00 (m, 12H), 0.89 (t, J = 8 Hz, 6H), 0.80-0.66 (m, 12H). HR-MS (MALDITOF) *m/z* calcd. for ($C_{82}H_{88}Cl_2N_8O_2S_5$): 1448.8595. Found: 1449.183.

Synthesis of 2,2'-((2Z,2'Z)-((12,13-bis(2-ethylhexyl)-3,9-diundecyl-12,13-dihydro-[1,2,5]thiadiazolo[3,4-e]thieno[2'',3'':4',5']thieno[2',3':4,5]pyrrolo[3,2-g]thieno[2',3':4,5]thieno[3,2-b]indole-2,10-diyl)bis(methanylylidene))bis(6-chloro-3-oxo-2,3-dihydro-1H-indene-2,1-diylidene))dimalononitrile (BTIC-2Cl-δ). Synthesis of **BTIC-2Cl-δ** was carried out in a similar manner to that of **BTIC-2Cl-γ**. ^{1}H NMR (400 MHz, $CDCl_3$) δ: 9.17 (s, 2H), 8.67 (d, *J* = 4 Hz, 2H), 7.87 (d, *J* = 8

Hz, 2H), 7.12 (dd, *J* = 8 Hz, 2H), 4.76 (d, *J* = 8 Hz, 4H), 3.23 (t, *J* = 8 Hz, 4H), 2.14-2.09 (m, 2H), 1.92-1.84 (m, 4H), 1.53-1.41 (m, 4H), 1.39-1.15 (m, 38H), 1.09-0.99 (m, 12H), 0.86 (t, *J* = 8 Hz, 6H), 0.77-0.54 (m, 14H). HR-MS (MALDITOF) *m/z* calcd. For ($C_{82}H_{88}Cl_2N_8O_2S_5$): 1448.8595. Found: 1449.223.

Synthesis of 2,2'-((2Z,2'Z)-((12,13-bis(2-ethylhexyl)-3,9-diundecyl-12,13-dihydro-[1,2,5]thiadiazolo[3,4-e]thieno[2'',3'':4',5']thieno[2',3':4,5]pyrrolo[3,2-g]thieno[2',3':4,5]thieno[3,2-b]indole-2,10-diyl)bis(methanylylidene))bis(4-chloro-3-oxo-2,3-dihydro-1H-indene-2,1-diylidene))dimalononitrile (BTIC-2Cl-β). Synthesis of **BTIC-2Cl-β**was carried out in a similar manner to that of **BTIC-2Cl-γ**. ^{1}H NMR (400 MHz, $CDCl_3$) δ:9.23 (s, 2H), 8.73-8.69 (m, 2H), 7.72-7.69 (m, 4H), 7.12 (dd, *J* = 8 Hz, 2H), 4.88-4.76 (m, 4H), 2.27 (t, *J* = 6 Hz, 4H), 2.15-2.09 (m, 2H), 1.95-1.87 (m, 4H), 1.54-1.50 (m, 4H), 1.42-1.38 (m, 4H), 1.35-1.17 (m, 28H), 1.08-0.99 (m, 12H), 0.89 (t, *J* = 8 Hz, 6H), 0.78-0.67 (m, 12H). HR-MS (MALDITOF) *m/z* calcd. for ($C_{82}H_{88}Cl_2N_8O_2S_5$): 1448.8595. Found: 1448.6519.

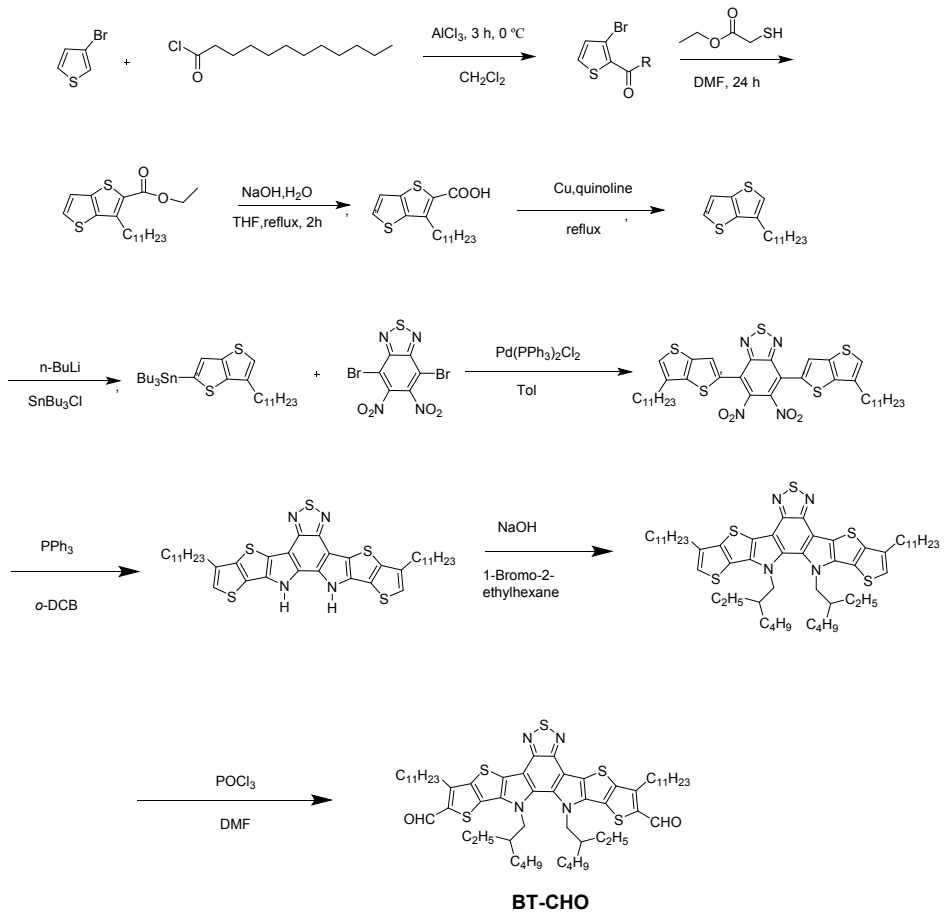

Figure S1. Synthetic routes of **BT-CHO**.

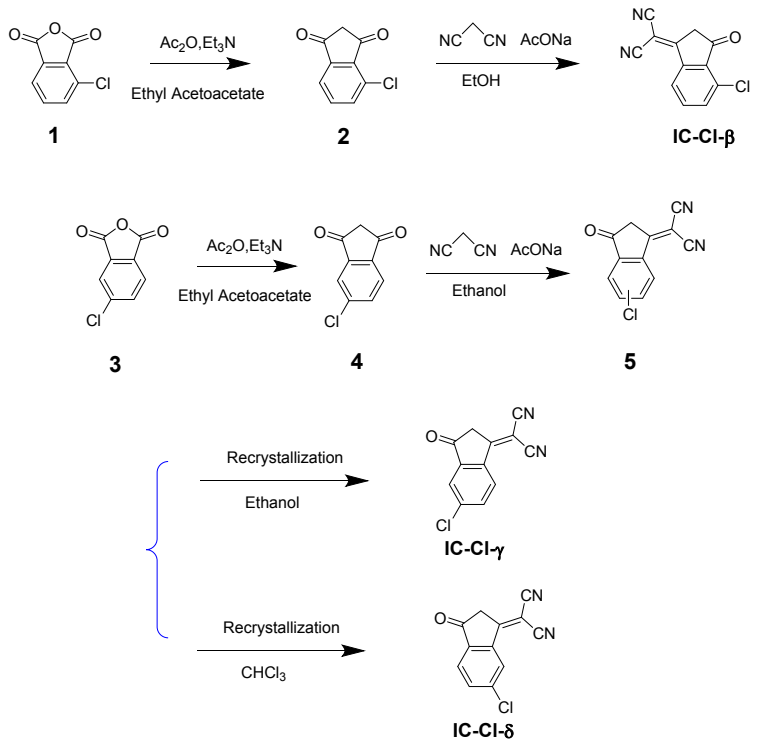

Figure S2. Synthetic routes of **IC-Cl-β**, **IC-Cl-γ**, and **IC-Cl-δ**.

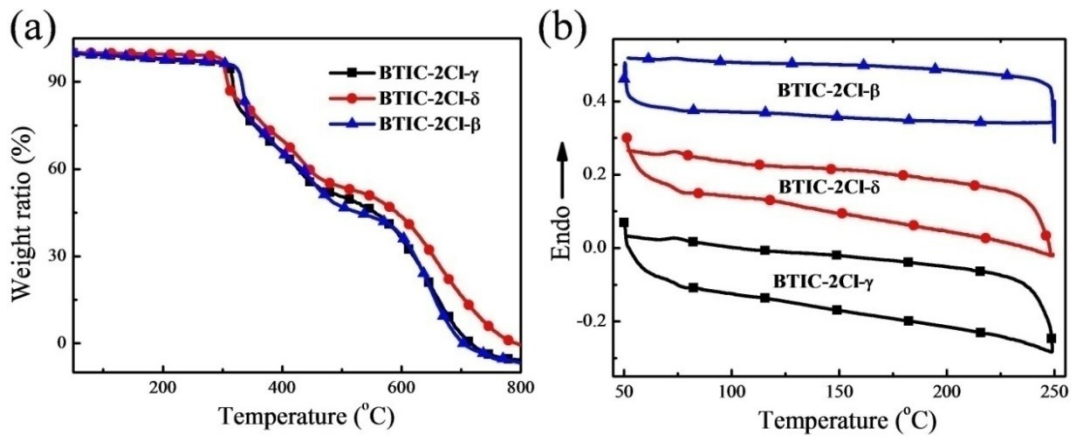

Figure S3. Thermogravimertic analysis (a) and differential scanning calorimetry (b) of **BTIC-2Cl-γ**, **BTIC-2Cl-δ**, and **BTIC-2Cl-β** at a heating/cooling rate of 10 °C min^{-1} in N_2.

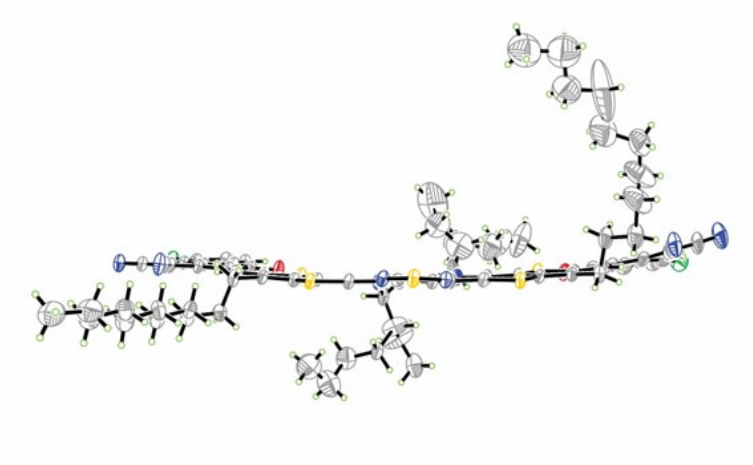

Figure S4. Single crystal structure of **BTIC-2Cl-δ** (side view).

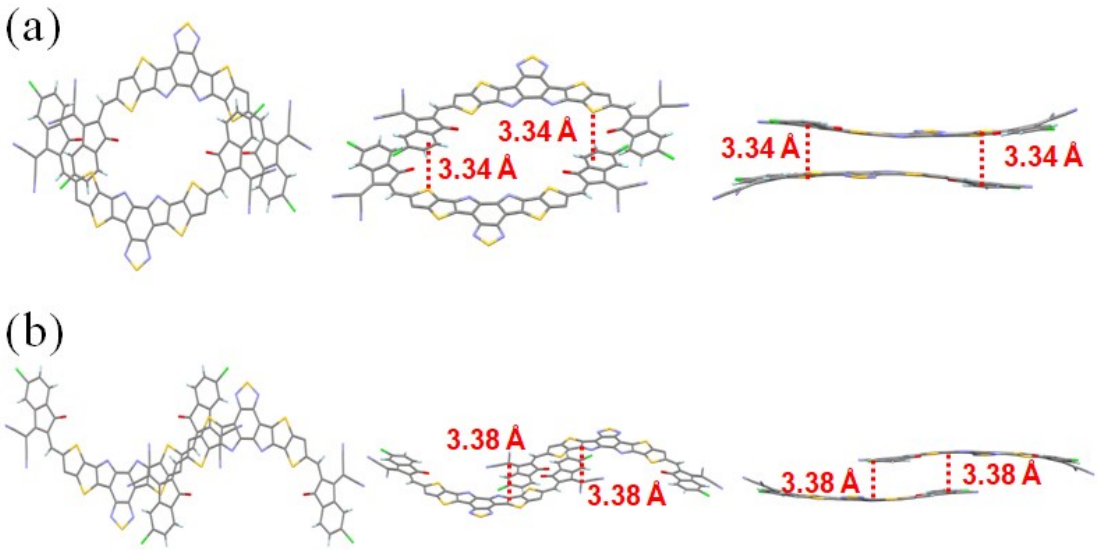

Figure S5. X-ray crystal structures of **BTIC-2Cl-δ**.

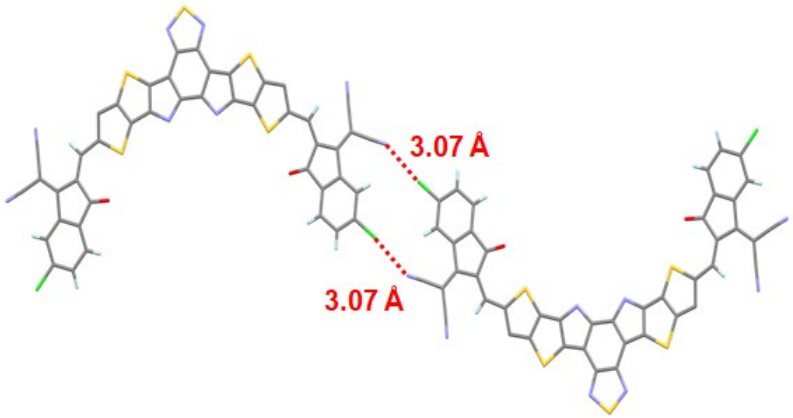

Figure S6. The Cl···N interactions of **BTIC-2Cl-δ**.

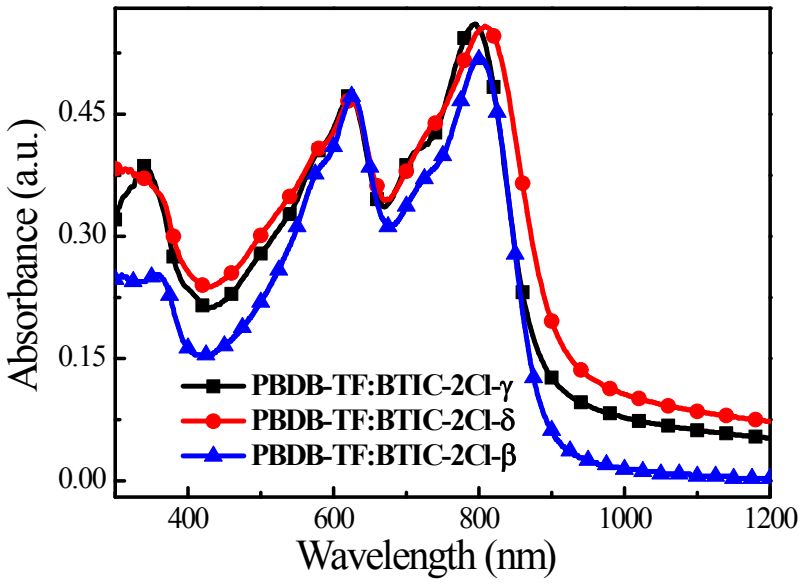

Figure S7. Absorption spectra of the PBDB-TF: **BTIC-2Cl-γ**, PBDB-TF: **BTIC-2 Cl-δ** and PBDB-TF: **BTIC-2Cl-β** blends films.

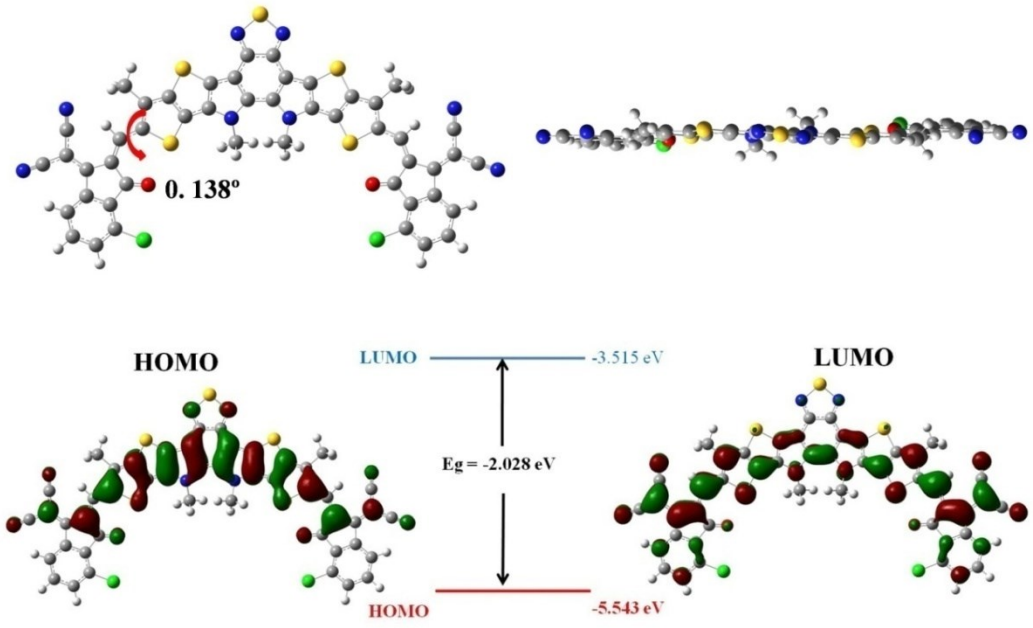

Figure S8. Optimized geometries and calculated molecular orbital of **BTIC-2Cl-β**.

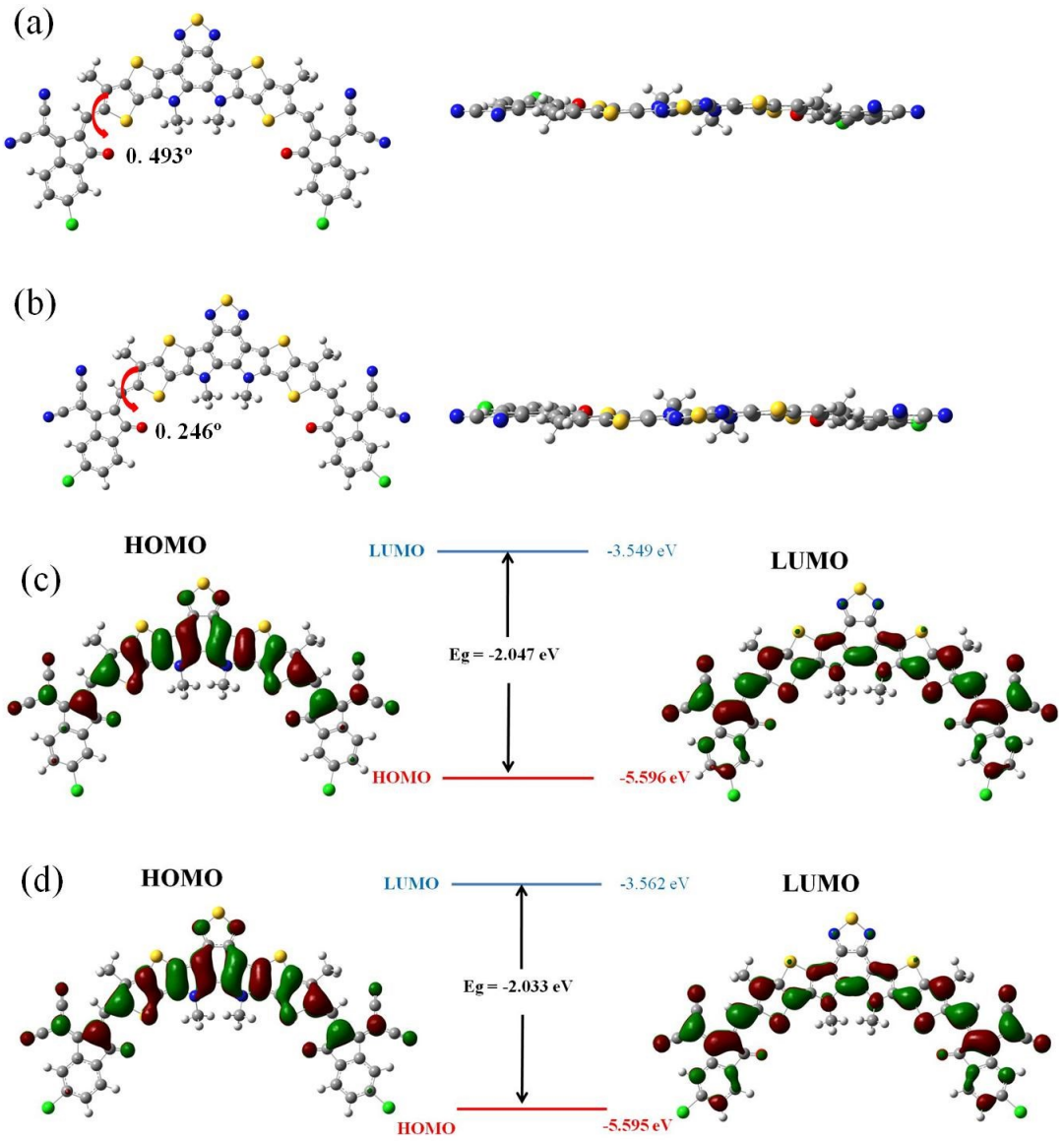

Figure S9. Optimized geometries and calculated molecular orbital of **BTIC-2Cl-γ** and **BTIC-2Cl-δ**.

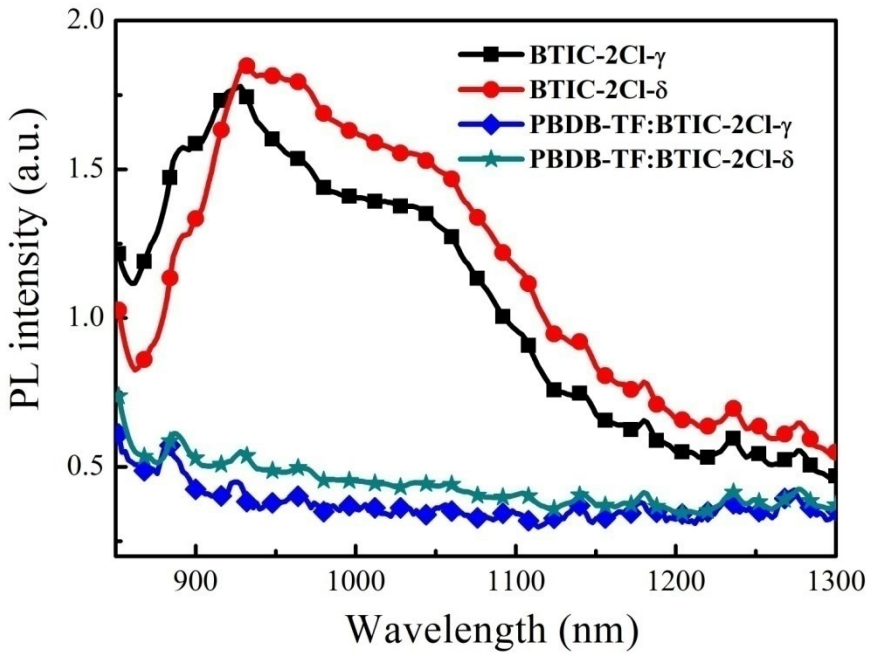

Figure S10. Photoluminescence (PL) spectra of **BTIC-2Cl-γ**, **BTIC-2Cl-δ**, and PBDB-TF: **BTIC-2Cl-γ** blend films and PBDB-TF: **BTIC-2Cl-δ** blend films, the excitation wavelength are 808 nm.

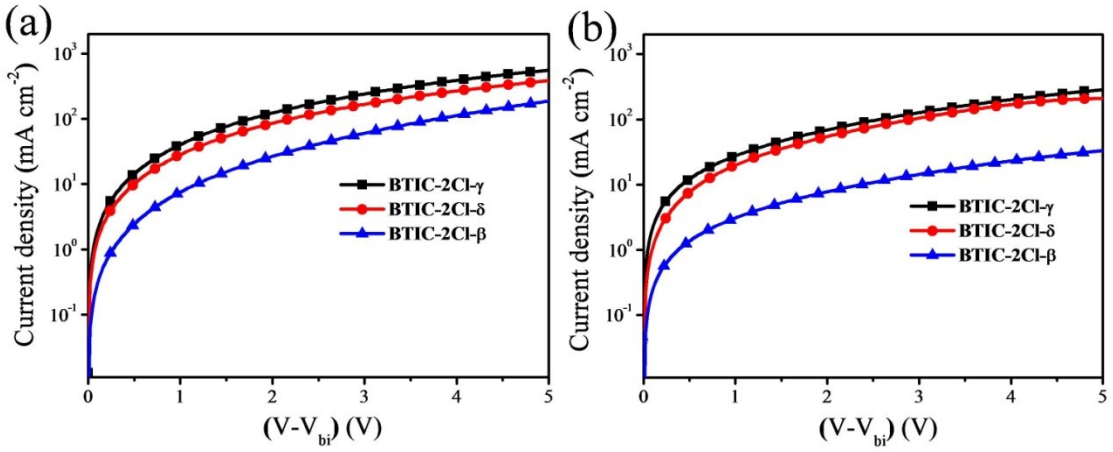

Figure S11. The *J-V* curves of the hole-only (a) and electron-only (b) of **BTIC-2Cl-γ**, **BTIC-2Cl-δ**, and **BTIC-2Cl-β**-based devices.

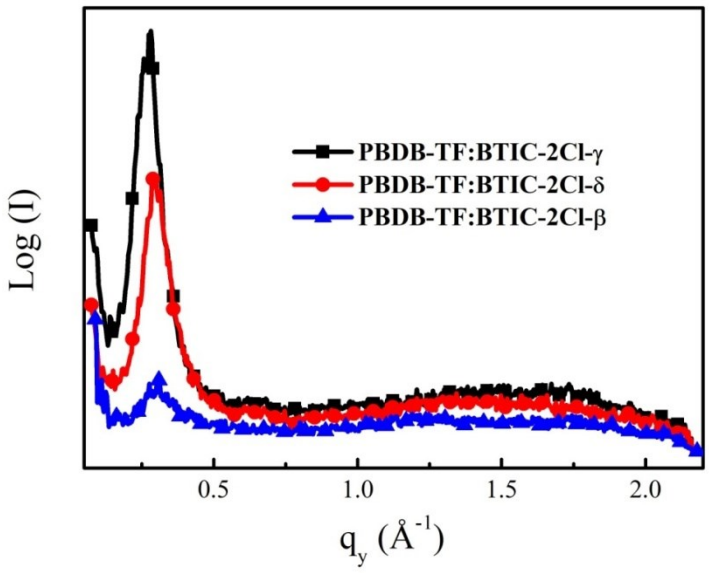

Figure S12. GIWAX line cuts of the in-plane among the blend films.

Table S1. The mobility data of the isomeric chlorinated acceptors.

Acceptors	Hole Mobility ($cm^2 v^{-1} s^{-1}$)	Electron Mobility ($cm^2 v^{-1} s^{-1}$)	Hole/Electron
BTIC-2Cl-γ	1.4×10^{-4}	9.5×10^{-5}	1.5
BTIC-2Cl-δ	9.2×10^{-5}	6.7×10^{-5}	1.4
BTIC-2Cl-β	2.7×10^{-5}	1.3×10^{-5}	2.1

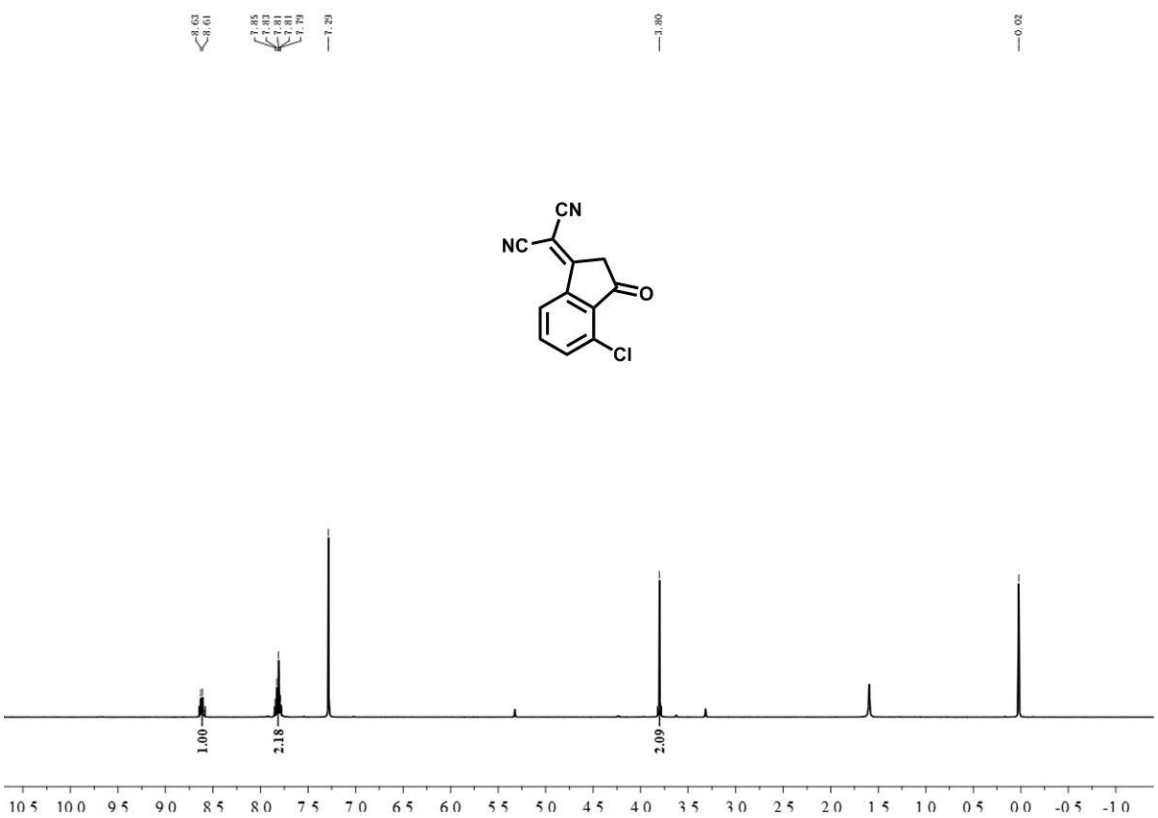

Figure S13. ^{1}H NMR of IC-Cl-β in $CDCl_3$.

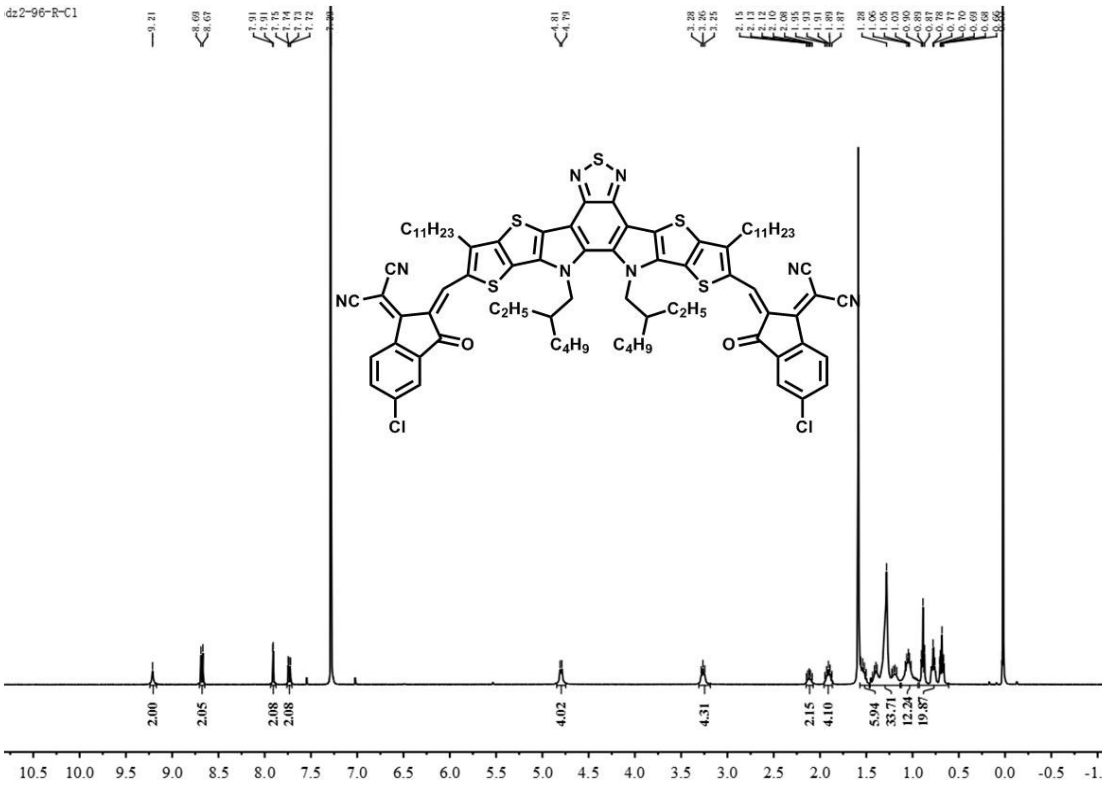

Figure S14. ^{1}H NMR of **BTIC-2Cl-γ** in $CDCl_3$.

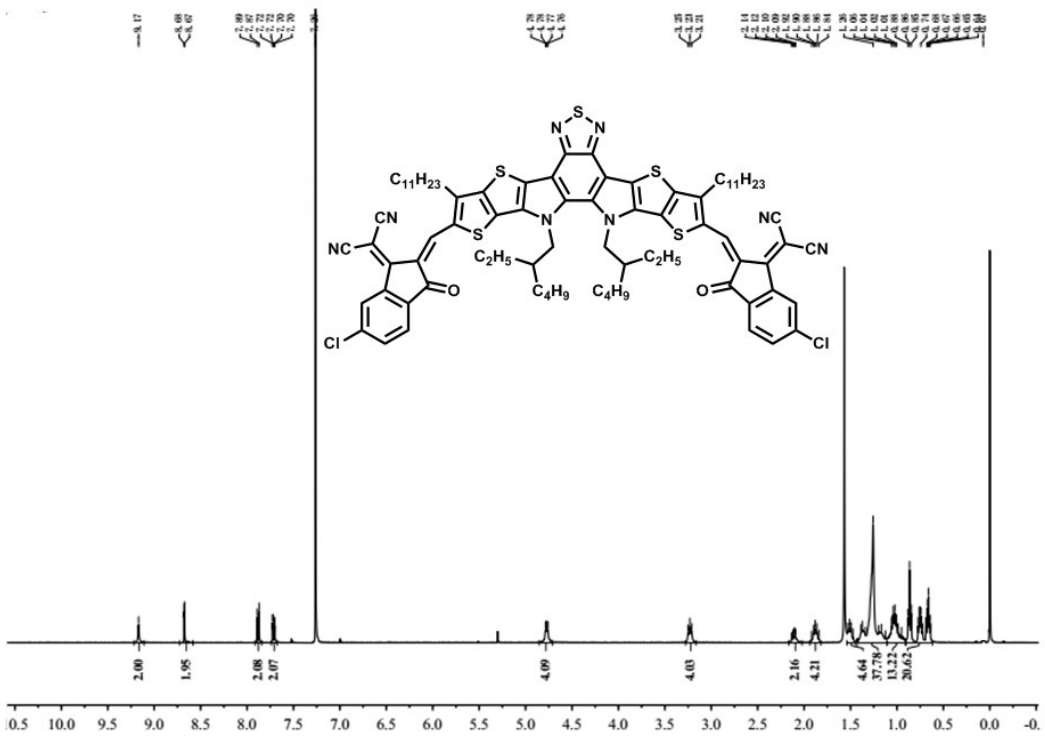

Figure S15. ^{1}H NMR of **BTIC-2Cl-δ** in $CDCl_3$.

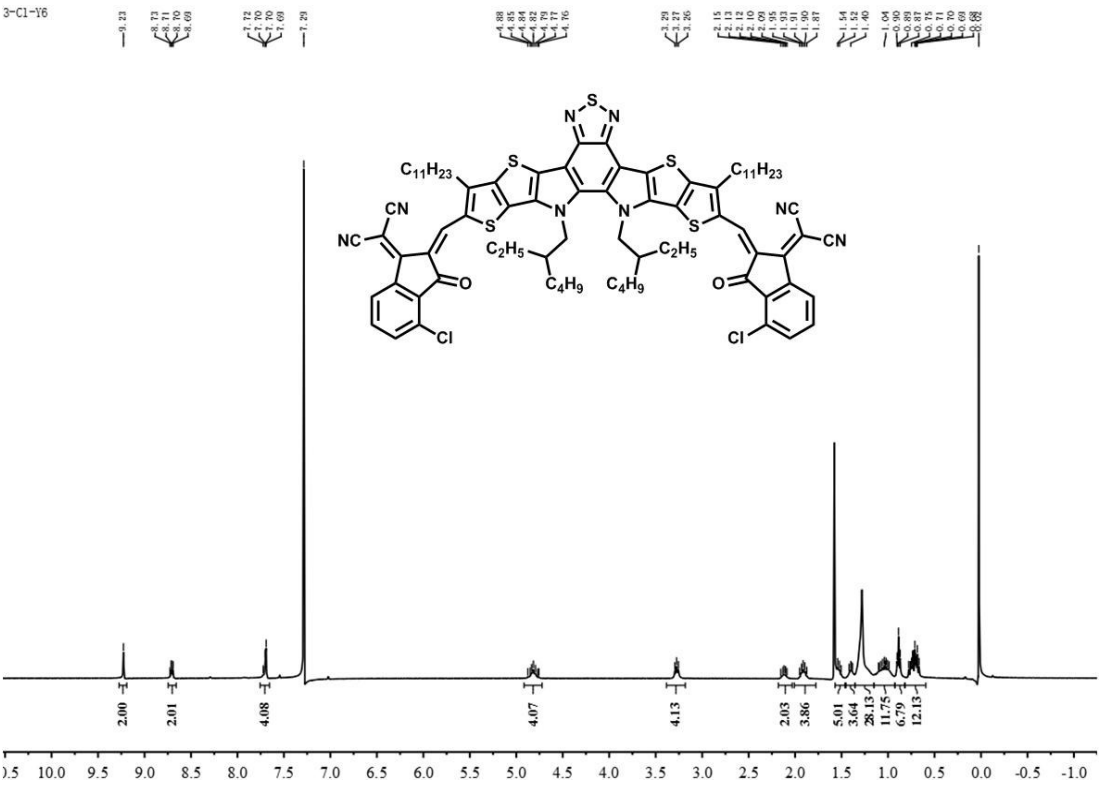

Figure S16. ^{1}H NMR of **BTIC-2Cl-β** in $CDCl_3$.

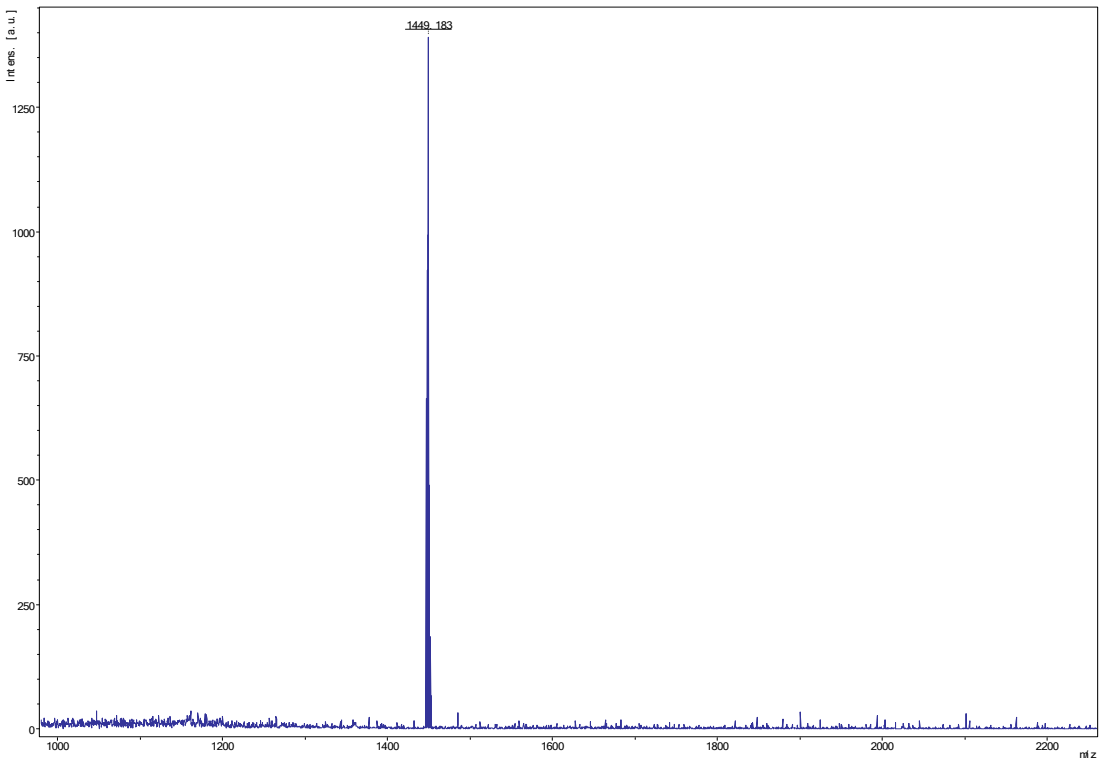

Figure S17. MS-MALDI spectra of **BTIC-2Cl-γ**.

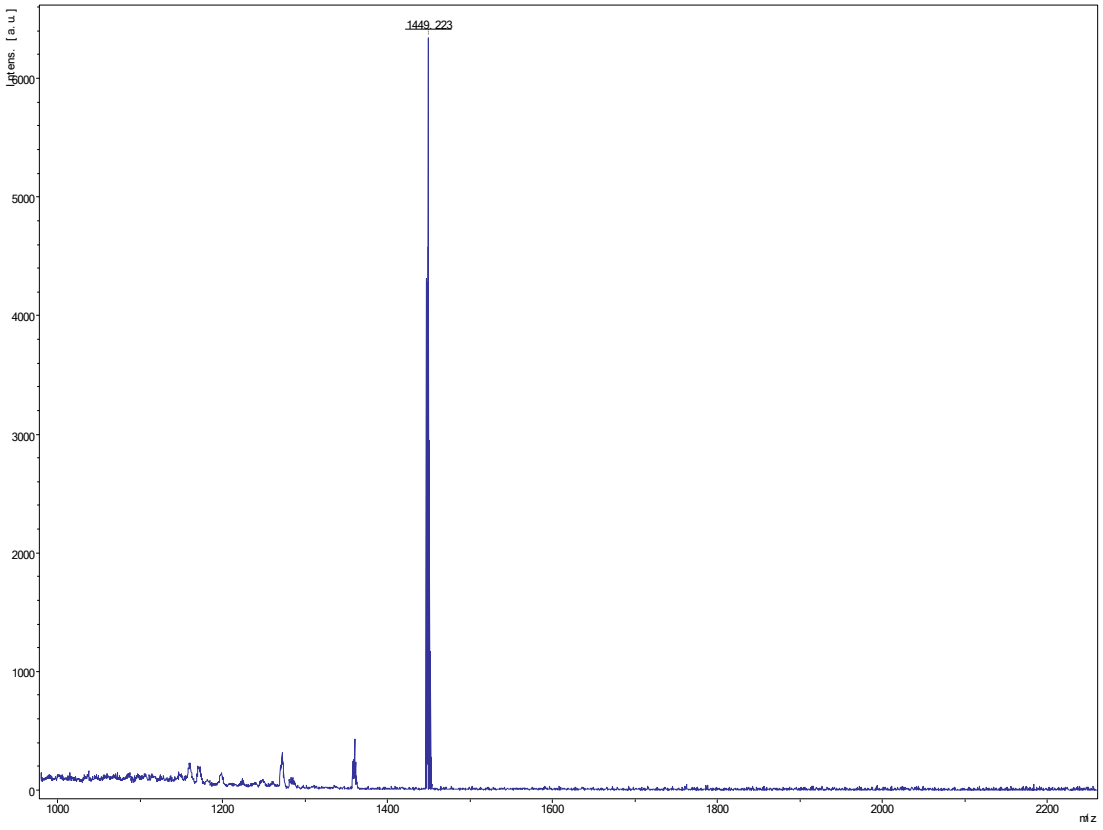

Figure S18. MS-MALDI spectra of **BTIC-2Cl-δ**.

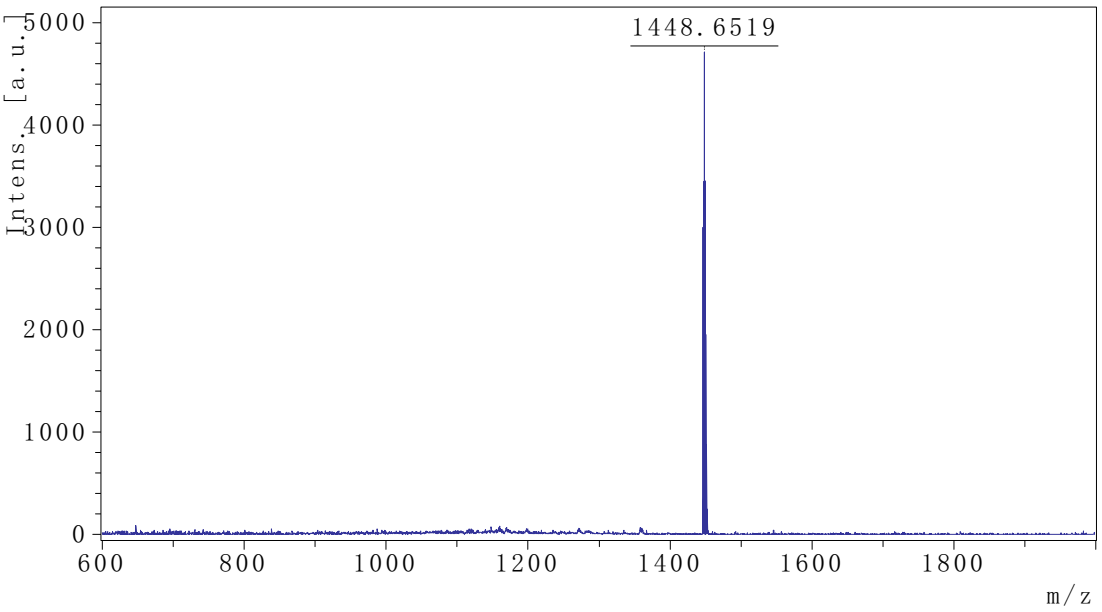

Figure S19. MS-MALDI spectra of **BTIC-2Cl-β**.

References in Supporting Information

1. D.Z. Mo, H. Chen, J.D. Zhou, N.N. Tang, L.Han, Y.L.Zhu, P.J. Chao,H.J. Lai, Z.Q.Xie and F.He. *J. Mater. Chem. A*., 2020, **8**, 8903-8912.

2. H.J. Lai, H. Chen, J.D. Zhou, J.F.Qu,P.J. Chao, T.Liu, X.Y. Chang,N.Zheng,Z.Q. Xie and F. He. *iScience* 2019, **17**, 302-314.

3. T. Liu, Q.Q. Zhao, H. Wang, J.F. Qu, P.J. Chao, N. Zheng, H.J. Lai, D.Z. Mo and F. He. *Mater. Chem. Front*., 2019, **3**, 1859-1865.